Appl. Phys. B (2015) 120:117–122
DOI 10.1007/s00340-015-6110-4

Applied Physics B
Lasers and Optics

Generation of visible wavelength by the phase-matching four-wave mixing in an Yb-doped V-shape photonic crystal fiber

Lixiao Li[1] · Jinhui Yuan[1] · Xinzhu Sang[1] · Binbin Yan[1] · Kuiru Wang[1] · Chongxiu Yu[1] · Ying Han[2] · Changming Xia[3] · Guiyao Zhou[2,3] · Shuai Wei[1] · Chao Wang[2] · Jianju Yang[2] · Shuang Wang[2] · Xu Cheng[1] · Lantian Hou[2]

Received: 8 July 2014 / Accepted: 11 April 2015 / Published online: 22 April 2015

Abstract In this paper, an Ytterbium-doped V-shape photonic crystal fiber (Yb-VPCF) with low dispersion and high nonlinearity is designed and fabricated in our laboratory. Through coupling femtosecond pulses into the fundamental mode of Yb-VPCF, the tunable anti-Stokes signals at the visible wavelength are efficiently generated based on the phase-matching four-wave mixing. When the pump wavelength is changed from 810, to 820, and to 830 nm and the input average power is increased from 0.4, to 0.5, and to 0.6 W, respectively, the anti-Stokes signals are generated within the wavelength range of 562–477 nm. The wavelength-tunable range is over 100 nm, and the maximum power ratio of anti-Stokes signal at 477 nm and the residual pump at 830 nm can be up to 23.9:1. The anti-Stokes signals generated can be used as the ultrashort pulse sources for ultrafast optoelectronics and spectroscopy.

1 Introduction

The development of photonic crystal fibers (PCFs) [1–3] has opened a new window for nonlinear optics [4–6] owing to their unique optical properties, such as endlessly single-mode, controlled dispersion, and high nonlinearity. Lots of researches have been focused on the nonlinear applications based on PCFs, which are fabricated by silica [7–9], bismuth oxide glass [10, 11], chalcogenide glass [12, 13], and heavy metal oxide glass [14]. In the communication network, the wavelength conversion techniques can be used for providing the wavelength flexibility and avoiding the wavelength block in the wavelength-division-multiplexing (WDM) system [10]. In particular, the efficient generation of anti-Stokes signals as a promising technique is extensively studied to generate the short wavelength radiations for the high-resolution imaging, multi-photon ionization, as well as preparation of vibrational wave packets [15], and so on.

Recently, the generation of anti-Stokes signals based on the phase-matching four-wave mixing (FWM) in the silica PCFs have been widely studied [16–22]. However, there are few reports on the generation of anti-Stokes signals in non-silica PCFs. Although the PCFs fabricated by other glass materials may suffer from large group-velocity dispersion and high absorption loss, they can show extremely low dispersion and high nonlinearity, which are particularly important for achieving efficient wavelength conversion within a wide wavelength range [23].

In this paper, an Ytterbium-doped V-shape PCF (Yb-VPCF) with low dispersion and high nonlinearity is designed and fabricated in our laboratory. The anti-Stokes signals are efficiently generated within the wavelength range of 562–477 nm through coupling femtosecond pulses into the fundamental mode of Yb-VPCF. The wavelength-tunable range is over 100 nm, and the maximum power ratio of the anti-Stokes signal at 477 nm to the residual pump at 830 nm can be up to 23.9:1.

✉ Jinhui Yuan
yuanjinhui81@163.com

[1] State Key Laboratory of Information Photonics and Optical Communications, Beijing University of Posts and Telecommunications, 100876 Beijing, China

[2] Institute of Infrared Optical Fibers and Sensors, Physics Department, Yanshan University, 066004 Qinhuangdao, China

[3] Guangdong Provincial Key Laboratory of Nanophotonic Functional Materials and Devices, South China Normal University, 510006 Guangzhou, China

2 Yb-VPCF properties and experiment

The cross section of Yb-VPCF used in the experiment is shown in Fig. 1a. The mode property can be analyzed by the full-vector finite element method (FV-FEM). The structure parameters are chosen as following: The average diameter of large air hole $D = 4.8$ μm, the average diameter of small air hole $d = 0.8$ μm, and the hole to hole pitch $\Lambda = 5.4$ μm. The V-shaped structure is introduced to obtain the low and flat dispersion within the considered wavelength range of 400–1500 nm, as shown in Fig. 1b. The dispersion curves along the *x*- and *y*-axis direction of Yb-VPCF are very close because the size of air holes in the first layer is very small and the induced birefringence is very low. As seen from the inset of Fig. 1b, the zero-dispersion wavelengths along the *x*- and *y*-axis direction are located at 862.6 and 865.7 nm, respectively. And a round Yb^{3+}-doped silica core is used to enhance the nonlinearity. The concentration of Yb^{3+} in the core region is ~10^3 ppm, which is much lower than that of ytterbium-doped PCF (~10^4 ppm) used for lasers. Figure 1c shows the effective mode area curves of Yb-VPCF and pure silica VPCF, where the values of Yb-VPCF and pure silica VPCF along the *x*-axis direction are changed from 5.05 to 9.9 and from 43.03 to 55.1 μm^2, respectively, within the wavelength range of 0.5–1.4 μm. Compared with the pure silica VPCF, the effective mode area of Yb-VPCF is decreased by 87 %, and the nonlinearity of Yb-VPCF can be greatly enhanced because the optical field energy is strongly confined in the core region.

As demonstrated in Refs [24, 25], when the strong pump pulses at the center frequency of ω_p are launched into a fiber, the anti-Stokes signals with the up-shifted frequency of ω_{as} and the Stokes signals with the down-shifted frequency of ω_s can be generated. The phase-matching condition $\kappa = \beta(\omega_{as}) + \beta(\omega_s) - 2\beta(\omega_p) + 2n_2\omega_p P_p/(cA_{eff}) = 0$ should be satisfied to achieve the energy transfer from the pump to the anti-Stokes and Stokes signals, where $\beta(\omega_{as})$, $\beta(\omega_s)$, and $\beta(\omega_p)$ are the propagation constants of the anti-Stokes signal, Stokes signal, and pump, P_p is the pump peak power, n_2 is the nonlinear refractive index, c is the light velocity in vacuum, and $A_{eff} = (\iint |E^2| dxdy)^2/(\iint |E^4| dxdy)$ is the effective mode area.

The phased-matching case can be affected by the material, waveguide structure, and nonlinearity effect. It is known that the phase-mismatching induced by the material can be well compensated by those resulting from the waveguide structure and nonlinear effect. Thus, the Yb-VPCF structure is designed to satisfy the phase-matching condition at the specific frequency. When the nonlinear term is neglected, the approximate

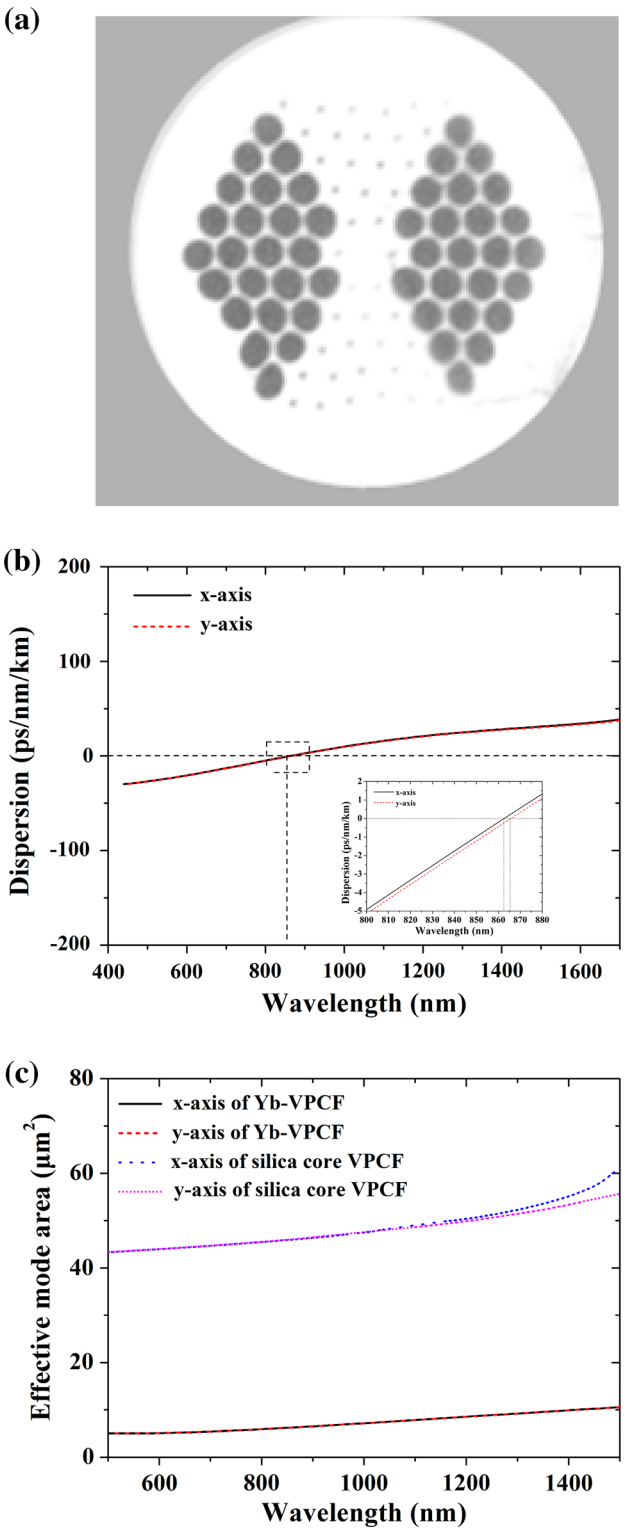

Fig. 1 **a** Cross section of Yb-VPCF used in the experiment, **b** group-velocity dispersion for the fundamental mode of Yb-VPCF, the *inset* showing the zoomed dispersion curves, and **c** the effective mode area curves of Yb-VPCF and pure silica VPCF along the *x*- and *y*-axis direction

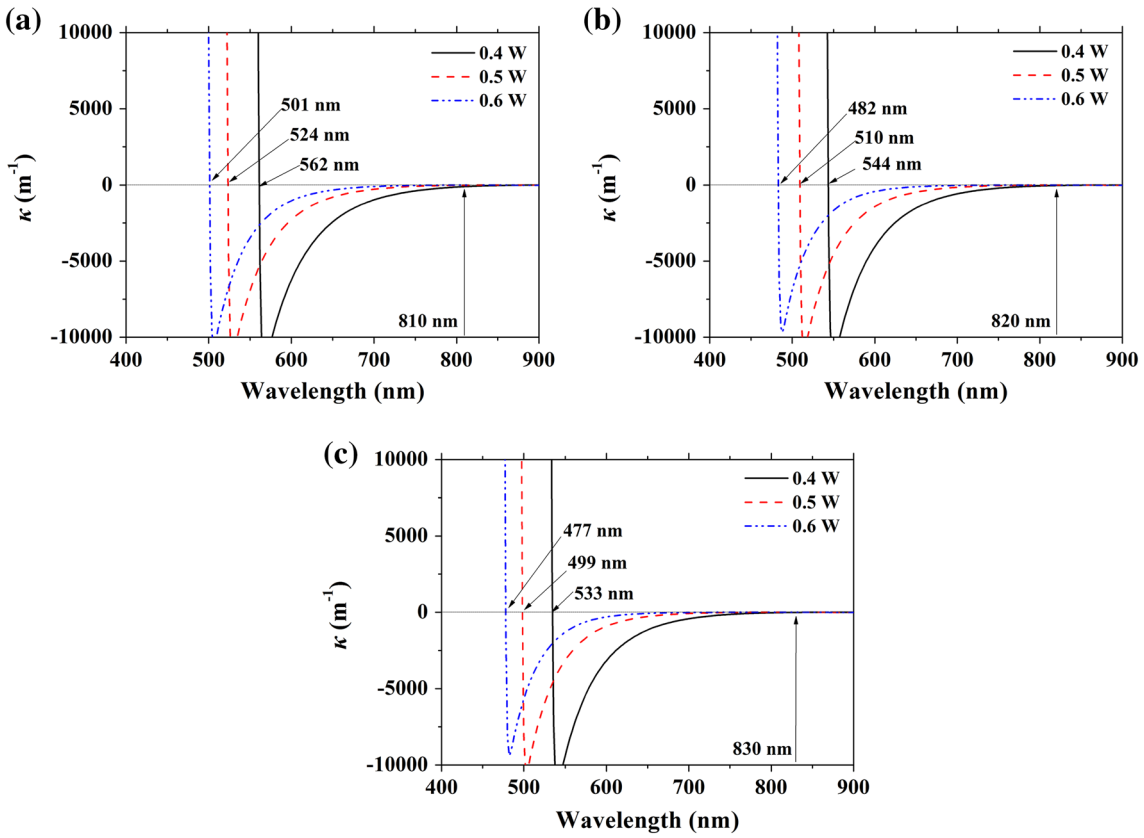

Fig. 2 Phase-mismatching curves at the short wavelength for the fundamental mode of Yb-VPCF as a function of radiation wavelength under different pump wavelengths and powers, and the *vertical arrow-lines* correspond to the pump wavelengths

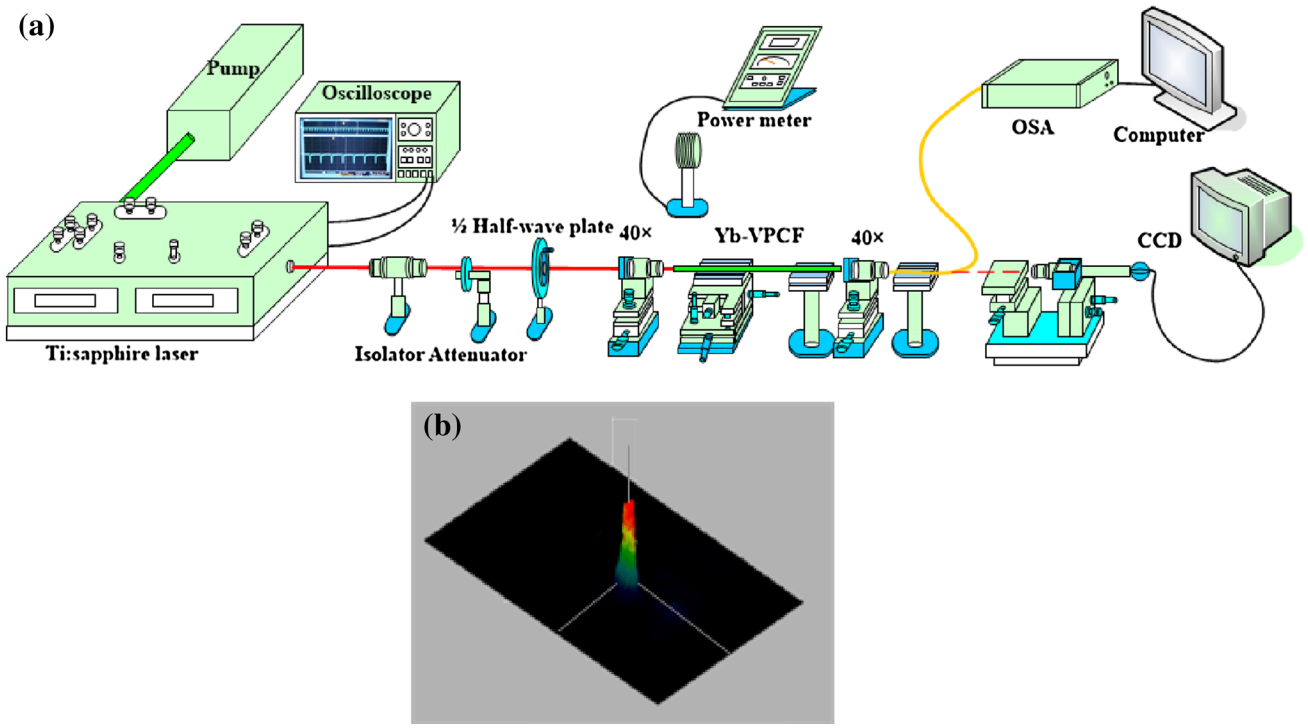

Fig. 3 **a** Experimental principle chart, and **b** the coupling state of input pump beam

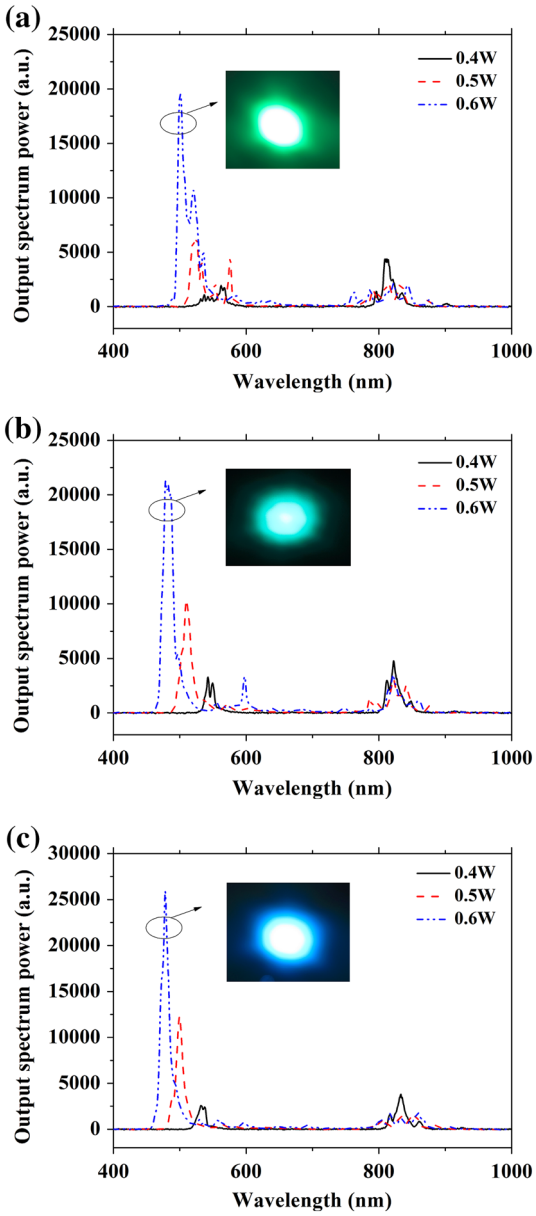

Fig. 4 Observed output spectra when the pump works at 810, 820, and 830 nm and the input average power increases from 0.4, to 0.5, and to 0.6 W, respectively. The *insets* show the observed output far fields with the *green*, *green–blue*, and *blue light* at 501, 482, and 477 nm

frequency relations between the Stokes wave, anti-Stokes wave, and pump wave can be described as follows: $\omega_{s,as} = \omega_p \mp \sqrt{-\beta^{(2)}(\omega_p)/\left[12\beta^{(4)}(\omega_p)\right]}$. Here, $\beta^{(n)}(\omega) = \partial^n \beta(\omega)/\partial\omega^n$ and the signs of $\beta^{(2)}(\omega_p)$ and $\beta^{(4)}(\omega_p)$ should be opposite for the phase-matching to occur.

Figure 2a–c shows the phase-mismatching curves of Yb-VPCF at the short wavelength as a function of radiation wavelength for different pump wavelengths and input average powers, the vertical arrow-lines corresponding to the pump wavelengths. As seen from them, when the pump works at 810, 820, and 830 nm and the input average power increases from 0.4, to 0.5, and to 0.6 W, the phase-mismatching parameter reaches zero at the wavelengths of 562, 524, and 501 nm; 544, 510, and 482 nm; 533, 499, and 477 nm, respectively, where the anti-Stokes signals will be remarkably generated.

The experimental setup is shown in Fig. 3a. The light source is a mode-locked Ti:sapphire laser, which has the center wavelength of 800 nm and emits a pulse train of 120 fs at the repetition rate of 76 MHz. The oscilloscope is used to display the mode-locked state of the laser pulses. An isolator is inserted to block the back-reflection from the input tip of the fiber into the laser cavity, and a variable attenuator is placed behind the laser to control the input powers. The 40× objective lens are used for adjusting the coupling efficiency. CCD is used to observe the coupling state of input pump field. The fiber alignment stage with a high precision is used to change the distance between the input tip of Yb-VPCF and the objective lens to adjust the angle between the input beam and the fiber axis (offset pumping technique), and the fundamental mode can be selectively excited. The optical beams are coupled into a 59-cm-long Yb-VPCF, and the coupling efficiency can be above 80 %, as shown in Fig. 3b. The output spectral properties can be monitored by the optical spectrum analyzer (OSA, Avaspec-256).

3 Results and discussion

The dependences of the observed output spectra on the radiation wavelength are shown in Fig. 4a–c when the input average power of pump pulses at 810, 820, and 830 nm increases from 0.4, to 0.5, and to 0.6 W, respectively. The corresponding insets show the output far fields observed at 501, 482, and 477 nm, whose transverse intensity distributions show the fundamental mode characteristics. In the initial stage of nonlinear dynamics, the self-phase modulation (SPM) plays an important role [26]. Frequency components near the zero-dispersion wavelength can serve as a pump for the phase-matching FWM involving the frequency-degenerate pump photos, which transfers the radiation energy of pump to the normal and anomalous dispersion regions. The anti-Stokes signals are efficiently generated within the wavelength range of 562–501, 544–482, and 533–477 nm, where the experimental results agree well with the theory ones as shown in Fig. 2a–c. And the wavelength-tunable range is over 100 nm (562–477 nm).

Figure 5a, b shows the output anti-Stokes signal wavelength and power as a function of the pump wavelength

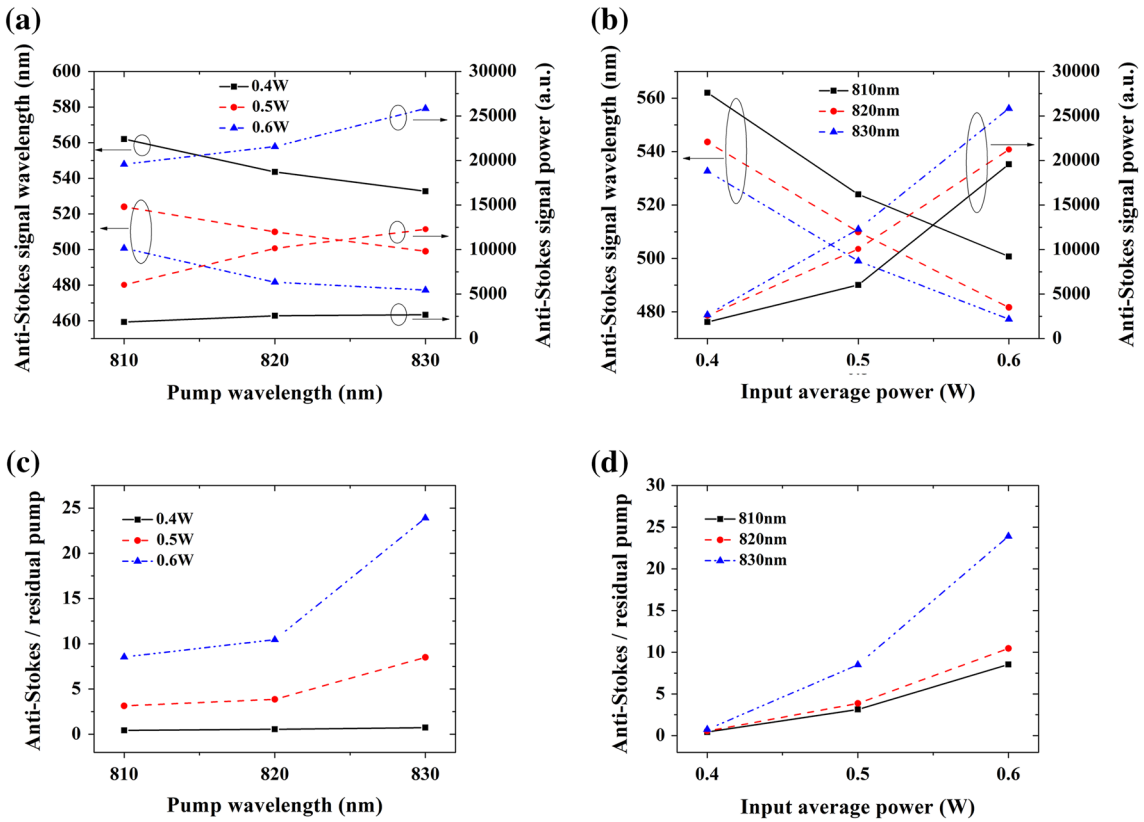

Fig. 5 **a**, **b** Output anti-Stokes signal wavelength and power as a function of the pump wavelength and the input average power, respectively, and **c**, **d** the power ratio of the anti-Stokes signals and the residual pump components as a function of the pump wavelength and the input average power, respectively

and the input average power, respectively. When the pump works at the determinate input average power and wavelength, the central wavelength and output power of anti-Stokes signal show the approximately linear functions of pump wavelength and input average power, respectively, but the changing trends are inverse. The larger slopes indicate that much higher wavelength-tunable sensitivity and conversion efficiency are achieved.

Figure 5c, d shows the output power ratio of the anti-Stokes signal and the residual pump component as a function of the pump wavelength and input average power, respectively. As seen from Fig. 5c, when the input average power is 0.4 W, the power ratio is changed slightly as the pump wavelength is increased from 810, to 820, and to 830 nm. At the same time, the power ratio is increased slowly as the input average power is increased from 0.4, to 0.5, and to 0.6 W at the pump wavelength of 810 nm compared to the pump wavelengths of 820 and 830 nm, as shown in Fig. 5d. When the wavelength interval between the pump wavelength and the zero-dispersion wavelength is smaller and the input average power is higher, the power ratio can be larger. Particularly when the input average power is 0.6 W, the output anti-Stokes signal powers are much higher than those of the residual pump components, and the power ratios of the anti-Stokes signals at 501, 482, and 477 nm and the residual pump components at 810, 820, and 830 nm are 8.5:1, 10.5:1, and 23.9:1. The anti-Stokes radiation contains above 80 % of the total output power calculated from the Manley–Rowe relations of photon conservation. In addition, it can be known from Figs. 4 and 5 that the input average power and wavelength interval are two crucial factors, which have great effects on the nonlinear process of anti-Stokes signal conversion.

4 Conclusions

In summary, the efficient conversion of anti-Stokes signals at the visible wavelength based on the phase-matching FWM is achieved in an Yb-VPCF with low dispersion and high nonlinearity designed and fabricated in our laboratory. The influences of the pump average power and the pump wavelength on the process of nonlinear conversion are experimentally demonstrated. It can be expected that the anti-Stokes signals can be efficiently generated in a wide wavelength range through designing the Yb-VPCF

structure and doping the Ytterbium material. The anti-Stokes signals generated can be used as the ultrashort pulse sources for ultrafast optoelectronics and spectroscopy.

Acknowledgments This work is partly supported by the National Natural Science Foundation of China (61307109 and 61475023), the Beijing Natural Science Foundation (4152037), the Specialized Research Fund for the Doctoral Program of Higher Education (20120005120021), the Fundamental Research Funds for the Central Universities (2013RC1202), the Fund of State Key Laboratory of Information Photonics and Optical Communications (BUPT) of China, the Hong Kong Scholars Program 2013 (PolyU G-YZ45), and the Research Grant Council of the Hong Kong Special Administrative Region China (PolyU5272/12E).

Conflict of interest We have no conflict of interest.

References

1. P.St.J. Russell, Science **299**, 358 (2003)
2. J.C. Knight, Nature **424**, 847 (2003)
3. P.St.J. Russell, J. Lightwave Technol. **24**, 4729 (2006)
4. N. Nishizawa, T. Goto, IEEE J. Sel. Top. Quantum Electron. **7**, 518 (2001)
5. K. Saitoh, M. Koshiba, Opt. Express **12**, 2027 (2004)
6. A.B. Fedotov, E.E. Serebryannikov, A.A. Ivanov, L.A. Mel'nikov, A.V. Shcherbakov, D.A. Sidorov-Biryukov, ChK Sun, M.V. Alfimov, A.M. Zheltikov, Laser Phys. Lett. **3**, 301 (2006)
7. X.Z. Sang, P.K. Chu, C.X. Yu, Opt. Quantum Electron. **37**, 965 (2005)
8. A.M. Zheltikov, J. Opt. A: Pure Appl. Opt. **8**, S47 (2006)
9. W. Astar, C.-C. Wei, Y.-J. Chen, J. Chen, G.M. Carter, Opt. Express **16**, 12039 (2008)
10. K.K. Chow, K. Kikuchi, T. Nagashima, T. Hasegawa, S. Ohara, N. Sugimoto, Opt. Express **15**, 15418 (2007)
11. J.H. Lee, K.Y. Song, H.J. Yoon, J.S. Kim, T. Hasegawa, T. Nagashima, S. Ohara, N. Sugimoto, Opt. Lett. **34**, 2670 (2009)
12. J. Hu, C.R. Menyuk, L.B. Shaw, J.S. Sanghera, I.D. Aggarwal, Opt. Commun. **293**, 116 (2013)
13. B. Dabas, J. Kaushal, M. Rajput, R.K. Sinha, Appl. Opt. **50**, 5803 (2011)
14. K.M. Kiang, K. Frampton, T.M. Monro, R. Moore, J. Tucknott, D.W. Hewak, D.J. Richardson, H.N. Rutt, Electron. Lett. **38**, 546 (2002)
15. A.H. Zewail, Science **242**, 1645 (1988)
16. E.R. Andresen, H.N. Paulsen, V. Birkedal, J. Thogersen, S.R. Keiding, J. Opt. Soc. Am. B **22**, 1934 (2005)
17. X.W. Shen, C.X. Yu, X.Z. Sang, J.H. Yuan, Y. Han, C.M. Xia, L.T. Hou, F. Rao, M. Xia, X.L. Yin, Acta Phys. Sin. **61**, 044203 (2012)
18. J.H. Yuan, X.Z. Sang, C.X. Yu, Y. Han, G.Y. Zhou, S.G. Li, L.T. Hou, J. Lightwave Technol. **29**, 2920 (2011)
19. J.H. Yuan, X.Z. Sang, C.X. Yu, S.G. Li, G.Y. Zhou, L.T. Hou, IEEE J. Quantum Electron. **46**, 728 (2010)
20. J.H. Yuan, X.Z. Sang, C.X. Yu, X.J. Xin, G.Y. Zhou, S.G. Li, L.T. Hou, Appl. Phys. B **104**, 117 (2011)
21. H.L. Wang, Y.X. Leng, Z.Z. Xu, Y.H. Qi, Chin. Phys. Lett. **26**, 084201 (2009)
22. W. Wang, L.T. Hou, Z.L. Liu, G.Y. Zhou, Chin. Phys. Lett. **25**, 3682 (2008)
23. K. Inoue, H. Toba, IEEE Photon. Technol. Lett. **4**, 69 (1992)
24. G.P. Agrawal, *Nonlinear Fiber Optics* (Academic Press, San Diego, 2001)
25. A.V. Husakou, J. Herrmann, Appl. Phys. Lett. **83**, 3867 (2003)
26. J.H. Yuan, X.Z. Sang, Q. Wu, G.Y. Zhou, C.X. Yu, K.R. Wang, B.B. Yan, Y. Han, G. Farrell, L.T. Hou, Opt. Lett. **38**, 5288 (2013)